

# Phase-matched generation of highly coherent radiation in water window region

Lap V. Dao,<sup>1,4,\*</sup> Chris Hall,<sup>1,4</sup> Hoang L. Vu,<sup>1,4</sup> Khoung B. Dinh,<sup>1,4</sup> Eugenui Balaur,<sup>2,4</sup>  
Peter Hannaford,<sup>1,4</sup> and Trevor A. Smith<sup>3,4</sup>

<sup>1</sup>Centre for Atom Optics and Ultrafast Spectroscopy, Swinburne University of Technology, Melbourne, Victoria, Australia

<sup>2</sup>Department of Physics, La Trobe University, Melbourne, Victoria, Australia

<sup>3</sup>School of Chemistry, The University of Melbourne, Melbourne, Victoria, Australia

<sup>4</sup>Australian Research Council Centre of Excellence for Coherent X-Ray Science, Melbourne, Victoria, Australia

\*Corresponding author: [dvlap@swin.edu.au](mailto:dvlap@swin.edu.au)

Received 24 February 2012; revised 20 April 2012; accepted 15 May 2012;  
posted 16 May 2012 (Doc. ID 163651); published 20 June 2012

Highly coherent extreme ultraviolet radiation around the water window region ( $\sim 4.4$  nm) is generated in a semi-infinite helium gas cell using infrared pulses of wavelength 1300 nm, energy 2.5 mJ, duration 40 fs, and repetition rate 1 kHz. The pressure-squared dependence of the intensity and the almost-perfect Gaussian profile and low divergence of the high harmonic source indicate a phase-matched generation process. The spatial coherence of the source is studied using Young's double-slit measurements. © 2012 Optical Society of America

OCIS codes: 140.7090, 140.7240.

## 1. Introduction

Femtosecond laser-driven high-harmonic generation (HHG) has become an increasingly important source for the supply of coherent extreme-ultraviolet radiation and soft x-rays. Compared with synchrotrons and x-ray free-electron lasers, these table-top sources are small scale and highly versatile, and their resulting unique characteristic output can be tailored according to the experimental requirements for many applications in time-resolved studies of ultrafast dynamics in atomic [1,2], molecular [3–5], and solid state systems [6–8]; in extreme ultraviolet interferometry [9]; in plasma physics [10,11]; and in coherent diffractive imaging [12].

For biological applications, the generation of radiation in the “water window” region (4.4–2.3 nm, or 280–540 eV) is an attractive feature because in this wavelength range the radiation is not absorbed by

water and nitrogen while absorption due to carbon is strong. Intense ultrashort pulses in the water window wavelength region would allow the capture of images of live cells in a real environment, preserving structural information that may be lost during the sample's preparation process. This soft x-ray radiation can be used to perform various experiments with high spatial and temporal resolution. Thus, light sources in this wavelength region have been targeted by many researchers, including life scientists and physicists [13].

Through the use of 800 nm driving pulses, the generation of radiation with high photon flux below the 100 eV region by phase-matched [14] or quasi-phase-matched [15] HHG has been reported. The conversion efficiency is  $\sim 10^{-5}$  and reaches the absorption limit at photon energies of  $\sim 45$  eV when argon gas has been used [16]. The cutoff rule for the generated photon energy is  $h\nu_{\max} = I_p + 3.2U_p$ , where  $I_p$  is the ionization potential of the gas and  $U_p$  is the ponderomotive energy given by  $U_p \sim I_L \lambda_L^2$ , and  $I_L$

and  $\lambda_L$  are the intensity and wavelength, respectively, of the driving laser. Gases with high ionization energy, such as helium, have been used to obtain high-photon energy radiation. However, because the recombination cross-section of the atom decreases with increasing ionization energy, the efficiency of the HHG process decreases when small atoms, such as helium, are used. Furthermore, high laser intensity is needed for the generation of higher harmonic orders, which in turn leads to higher levels of ionization and therefore higher free electron dispersion. Efficient generation of high-order harmonics requires minimization of the phase mismatch between the harmonic and the driving laser fields. When a driving laser pulse at 800 nm is applied, phase matching of the HHG process can be achieved only at a low level of ionization of the medium, in order for the neutral atom dispersion to balance the anomalous free electron plasma dispersion [14]. Phase matching is possible only for ionization fractions below a critical level given by  $\eta_C(\lambda_L) = \{1 + \lambda_L^2 r_e N_{\text{atm}} / [2\pi \Delta n(\lambda_L)]\}^{-1}$  [21], where  $\eta$  is the ionization fraction,  $r_e$  is the classical electron radius,  $N_{\text{atm}}$  is the number density of atoms at 1 atm, and  $\Delta n$  is the difference between the refractive indices of the gas at the fundamental and harmonic wavelengths. When a short laser pulse ( $\sim 10$  fs) is used [18], a high laser field can be applied and the self-induced phase of the driving laser pulse can contribute to nonadiabatic self-phase matching. In this way, high photon energy can be generated, but the photon flux ( $\sim 10^6$  photons/s) in the water window region is not very high. For a long laser pulse ( $> 25$  fs), the cutoff energy for phase matching generation is much lower than the single atom cutoff. Even if quasi-phase matching or nonadiabatic self-phase matching is used, the conversion efficiency is low, that is, in the  $\sim 300$  eV region.

The  $\lambda_L^2$  scaling of the cutoff energy allows the generation of higher harmonic orders using long wavelength driving pulses. A significant extension of the cutoff energy has been demonstrated in several experiments using a gas jet [19] or hollow waveguide geometry [20–22]. The higher pressures of gas (up to 9 atm [22]) required for HHG using infrared (IR) wavelengths (compared with several tens or hundreds of Torr at 800 nm) is difficult to obtain in a free-space gas jet.

The development of high-energy, near-infrared laser systems based on optical parametric amplification (OPA) and/or optical parametric chirped-pulse amplification [23–27] has attracted considerable attention as a way to obtain high-power IR pulses. A total conversion efficiency of 20% for a three-stage barium borate type-II OPA at 1 kHz has been reported [24], and although conversion efficiencies as high as 45% for the final stage have been achieved, the total output energy was not higher than 1 mJ [23–25]. High-energy IR pulses, e.g., 7 mJ at 1.4  $\mu\text{m}$ , with 40 fs pulse width and 10 Hz repetition rate [26], or 1.5 mJ at 1.5  $\mu\text{m}$ , with 19.8 fs pulse width and

20 Hz repetition rate [27], have been achieved, but the repetition rate is still low.

In this paper, we report the use of a bismuth triborate ( $\text{BiB}_3\text{O}_6$ , or BIBO) nonlinear crystal to construct a high-power optical parametric amplifier pumped by 8 mJ pulses from a multipass Ti:sapphire amplifier at a 1 kHz repetition rate. High-energy (2.5 mJ) IR pulses at 1300 nm and with short duration ( $< 40$  fs) are used for phase-matched generation of radiation of high spatial coherence around the water window region in a semi-infinite cell filled with helium gas. Phase-matched generation is confirmed from studies of the pressure dependence. The coherence of the source is studied by measurements of the beam profile and the interference pattern from a Young double-slit (YDS) experiment.

## 2. Experiments and Results

BIBO is an interesting nonlinear optical crystal, because its second-order nonlinear susceptibility is high [28] and its low wavelength transparency edge extends into the UV at 286 nm. The high effective nonlinearity,  $d_{\text{eff}}$ , of BIBO allows the use of thin crystals. Thin crystals are used to avoid higher order nonlinear processes, which can become important in the generation of femtosecond IR pulses, and they also increase the transparency for a given crystal size. Different phase matching configurations can also be used, because BIBO is optically biaxial. It is preferable to use type-II interactions for a pump wavelength at 800 nm, which is possible in the  $x$ - $z$  principal plane, where BIBO acts as optically positive ( $oe \rightarrow o$  or  $oe \rightarrow e$  interaction, where “ $o$ ” represents the ordinary ray and “ $e$ ” the extraordinary ray) [29].

The output of a 1 kHz multistage, multipass, chirped-pulse amplifier system that produces 8 mJ pulses of 30 fs duration and centered at 810 nm is used to pump the OPA system. A collinear OPA scheme is used in our high-energy IR laser system in order to efficiently amplify the OPA signals. One third of the output of the multistage amplifier (2.5 mJ) pumps a commercial OPA (Quantronix, Palitra), which is designed with a two-stage configuration seeded by a white light continuum. The total efficiency (signal plus idler) of the Quantronix OPA is high ( $\sim 40\%$ ), but the pulse duration is long ( $> 300$  fs) because a long medium is used for generation of the white light. The remaining 5.5 mJ is used to pump the power amplifier stage. Type II crystals, cut at  $\theta = 42^\circ$  in the  $x$ - $z$  principal plane ( $\phi = 0$ ) for  $o \rightarrow eo$  interaction, have been used in all subsequent stages. The effective nonlinearity of BIBO for this type of interaction, e.g., assuming a signal wavelength  $\lambda_s = 1400$  nm, is  $d_{\text{eff}} = d_{12} \cos \theta = 2.38$  pm/V [29]. A type-II interaction has the advantage that it allows the possibility to tune, even close to degeneracy, at an almost constant bandwidth for the signal and idler. The signal and idler waves travel in opposite directions relative to the pump, which ensures exponential growth of the parametric gain even beyond the pulse walk-off length [30]. In the high-power OPA

stage, we employed a 2 mm thick BIBO crystal with an aperture of  $15 \times 15 \text{ mm}^2$ , which was placed about 50 cm away from the commercial OPA. The power amplifier OPA stage is seeded by the amplified signal from the commercial OPA, whose output is carefully adjusted for a collimated signal beam. The maximum conversion efficiency for the power amplifier stage was  $\sim 60\%$ , producing a total (signal and idler) output of  $\sim 4 \text{ mJ}$ . An IR pulse duration of 40 fs was measured by sum-frequency mixing with a 30 fs fundamental pulse.

The OPA output pulses at 1300 nm are focused by a 300 mm focal length fused silica lens into a 250 mm long gas cell with a 3 mm thick fused silica window at the entrance and a  $200 \mu\text{m}$  pinhole at the exit. The small exit pinhole is used to isolate the vacuum chamber from the gas-filled cell. The beam diameter at the focus is  $\sim 100 \mu\text{m}$  and the Rayleigh length is  $\sim 10 \text{ mm}$ . A similar experimental setup, but with an 800 nm driving pulse, has been reported elsewhere [31]. We use helium gas for HHG in the water window region because of its high ionization energy and because theoretical calculations [22] indicate that it is possible to obtain phase matching for the generation of radiation in the water window region using 1300 nm radiation. A very high gas pressure (up to 5 atm) is used for the generation of radiation of  $\sim 4.3 \text{ nm}$ . To maintain a low pressure in the vacuum chamber outside the gas cell, the experimental chamber has five different pumping stages separated by a series of pinholes. For optimal high harmonic intensity and beam profile, the position of the focus point relative to the exit pinhole can be varied and the diameter of an aperture, which is placed in the path of the laser beam before the focusing lens, can be controlled. A 300 nm thick aluminum filter with high transmission in the wavelength range  $< 5 \text{ nm}$  ( $\sim 10\%$  at 4 nm) and a 300 nm thick silver filter with transmission in the wavelength range 4–12 nm are used to remove the fundamental beam [32]. The high harmonic beam passes through a 0.5 mm wide, 20 mm high entrance slit of a commercial grazing incidence spectrometer (GIMS #4, Setpoint) before being dispersed by a 1200 lines/mm diffraction grating and detected by a back-illuminated extreme UV (XUV) charge-coupled device (CCD) camera. The far-field profile of the harmonic beam is detected directly by a  $13.3 \times 13.3 \text{ mm}$  CCD chip with pixel size  $13 \times 13 \mu\text{m}$  (PIXIS-XO-1024B, Roper Scientific). The HHG photon number  $N_{\text{ph}}$  is calculated from the signal from the CCD detector directly and after dispersion by the spectrometer using the expression  $N_{\text{ph}} = (N_c \eta / \text{QE}) \times (3.65 / E_{\text{ph}})$ , where  $N_c$  is the number of counts per CCD pixel,  $\eta$  depends on the setting of the hardware gain and is given by the manufacturers, QE is the quantum efficiency of the detector, which is nearly constant over the range of photon energies 20–350 eV, and  $E_{\text{ph}}$  is the photon energy.

One YDS configuration composed of two parallel slits  $4 \mu\text{m}$  wide,  $100 \mu\text{m}$  high, and with a slit separation

of  $20 \mu\text{m}$  is used for studies of the spatial coherence of the high harmonic beam. Two other YDS configurations composed of two parallel slits  $10 \mu\text{m}$  wide,  $100 \mu\text{m}$  high, and with slit separations of  $50 \mu\text{m}$  and  $75 \mu\text{m}$  are used to determine the spatial coherence. The YDS is located 1000 mm from the source. The interference fringes are detected by a CCD located 800 mm from the slit.

Figure 1 shows the XUV spectrum emitted from helium at different pressures with an exposure time of 20 s for each spectrum. Because the position of the focus of the driving laser beam is close to the exit pinhole of the gas cell, the HHG radiation is produced mostly in regions in the gas cell before the focal point along the axis of the fundamental beam. The bandwidth and beam profile of the HHG radiation depend on the gas pressure, the focus position, and the diameter of the fundamental beam. When the helium pressure is low ( $< 2 \text{ atm}$ ), the HHG radiation is observed at a wavelength of  $\sim 5 \text{ nm}$  and the beam divergence is large. HHG radiation above the carbon K-edge (4.4 nm) is obtained for gas pressures  $> 4 \text{ atm}$ . The beam profile is remarkably improved for pressures  $> 3 \text{ atm}$ . The intensity of the IR pulses ( $< 5 \times 10^{14} \text{ W/cm}^2$ ) is adjusted for low ionization of the gas ( $\eta < 1\%$ ) to generate high harmonic radiation from the neutral atoms. Through use of the 1300 nm driving field, the generated photon energy at the cut-off is approximately two times higher than when a 800 nm driving field is applied for a similar configuration.

Because the efficiency of HHG scales as  $\lambda^{-6.5}$  [33] for the effective generation of radiation with an IR source, it is necessary to increase the distance over which the harmonics interact constructively. Gas-filled hollow fibers have been used for enhancement of the interaction length [21,22]. In such a configuration, the pump laser can be guided to ensure a constant intensity over the length of the interaction, although the coupling of the strong field in the fiber will be limited. When a long focal length lens is used, self-guiding of the femtosecond pulses occurs as a

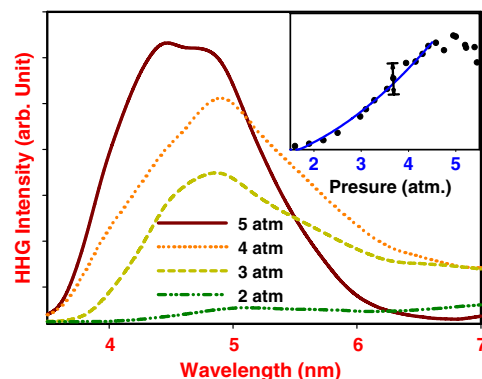


Fig. 1. (Color online) XUV HHG spectra from helium at different gas pressures. The inset shows the harmonic yield versus the gas pressure, the points show the experimental data, and the line represents the best fit with  $P^2$  (where  $P$  is the gas pressure).

result of beam convergence due to self-focusing and multiple photoionization [34]. This provides a relatively long interaction length with almost constant intensity of the driving field around the focus.

The number of photons for the  $q$ th harmonic  $N_{\text{out}}$  (the harmonic intensity) emitted on-axis per unit of time and area is given by [35]

$$N_{\text{out}} \sim \rho^2 A_q^2 \frac{4L_{\text{abs}}^2}{1 + 4\pi^2(L_{\text{abs}}^2/L_{\text{coh}}^2)} \left[ 1 + \exp\left(-\frac{L_{\text{med}}}{L_{\text{abs}}}\right) - 2 \cos\left(\frac{\pi L_{\text{med}}}{L_{\text{coh}}}\right) \exp\left(-\frac{L_{\text{med}}}{L_{\text{abs}}}\right) \right],$$

where  $\rho$  is the gas density,  $L_{\text{abs}}$  is the absorption length,  $L_{\text{med}}$  is the interaction length, and  $A_q$  is the atomic response.  $L_{\text{coh}} = \pi/\Delta k$  is the coherence length, where  $\Delta k$  is the total phase mismatch between the fundamental laser field and the harmonic field along the axis of the fundamental laser beam.

In the semi-infinite gas cell configuration, the aperture in front of the focus lens plays a very important role. Variation of the aperture in the input beam can be used to alter the spatial quality of the laser beam, the peak intensity in the focus area, and the ionization rate. This leads to a balance between the linear and nonlinear atom dispersion, the geometrical phase shift, and the plasma dispersion. The variation of the size of the laser beam also introduces a phase variation in the laser wavefront. This is why the size of the aperture plays a very important role in the minimization of the phase mismatch. If the generation of high-order harmonics is phase matched ( $\Delta k_q(z) \approx 0$ ) or the coherence length is long, the intensity of the harmonics scales as  $\rho^2$  or  $P^2$ , where  $P$  is the gas pressure. The inset in Fig. 1 shows the total photon number in the spectral range 4–5 nm for different gas pressures where a 300 nm thick Al foil has been used. In this case, the HHG signal is optimal for high flux and best beam profile at a gas pressure of 5 atm. The closed circles show the experimental data, and the solid line shows a fit based on  $P^2$ . For low pressures (<4 atm), the HHG signal increases quadratically with pressure, as is expected for phase-matched HHG emission. For high pressures (>5 atm), the phase mismatch is increased because of the high absorption.

Figure 2 shows the spatial profile of the HHG beam at a distance of 1800 mm from the source. The beam diameter was measured to be 0.8 mm (FWHM). As shown in this figure, the almost perfect Gaussian profile of the HHG beam suggests there is no density disturbance due to ionization in the interaction region. The observed dependence of the HHG output on pressure and the observed spatial profile indicate that macroscopic phase matching is satisfied along the propagation axis in our geometrical configuration. The photon flux around the maximum of the beam profile, measured by the CCD, in the wavelength range 4–5 nm is  $\sim 7 \times 10^7 - 10^8$  photons/cm<sup>2</sup>s when the transmission of the Al foil is assumed to be

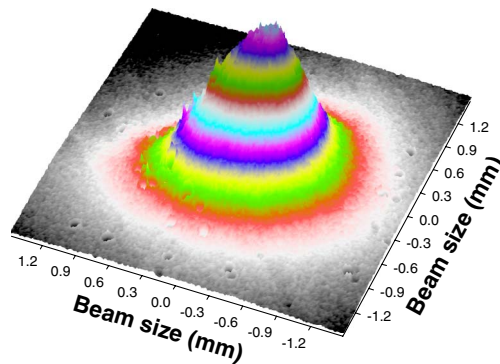


Fig. 2. (Color online) Beam profile of the radiation at a distance of 1800 mm from the source.

$\sim 10\%$ . The uncertainty of this measurement is high, because this wavelength range is close to the transmission edge of the Al foil, and thus small variations of foil thickness can influence the results.

To study the spatial coherence of the source in more detail, a YDS is used. Figure 3 shows a clear interference pattern resulting from the YDS that consists of two parallel slits 4  $\mu\text{m}$  wide, 100  $\mu\text{m}$  high, and with a 20  $\mu\text{m}$  separation. The beam diameter at the slit position is  $\sim 0.5$  mm (FWHM), which is much larger than the slit separation. When the gas pressure is high (>3.5 atm), the contrast at the center of the interference pattern is nearly independent of the gas pressure. We note that the YDS was illuminated from a broad wavelength beam (an Al foil was used to filter out the fundamental beam), and therefore the contrast of the fringes is not very high. The interference pattern is dependent on the gas pressure, indicating a variation of the harmonic spectrum with pressure. The observation of a high order of interference fringes and a very high signal-to-noise ratio indicates that the photon flux of our source is high (Fig. 3) compared with that in previous reports [19,22]. The width of the slits is small (4  $\mu\text{m}$ ) in our

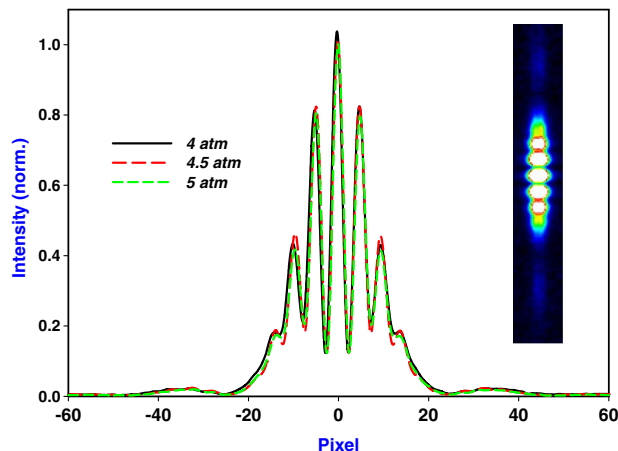


Fig. 3. (Color online) Interference fringes of YDS. The YDS consists of two parallel slits 4  $\mu\text{m}$  wide and 100  $\mu\text{m}$  high, and a 20  $\mu\text{m}$  separation. The CCD is located 800 mm from the slit. The inset shows the CCD image.

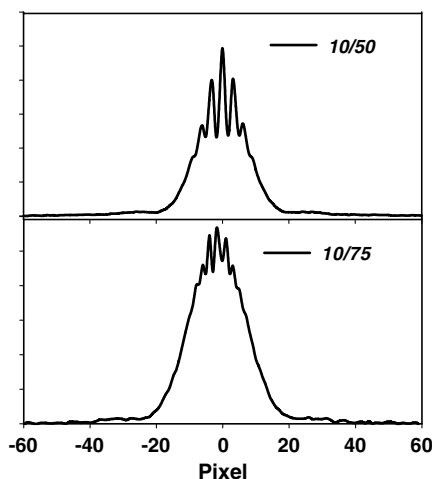


Fig. 4. Interference fringes of two YDSs with slit separations of 50  $\mu\text{m}$  and 75  $\mu\text{m}$ . The CCD is located 800 mm from the slit.

experiment, but the signal-to-noise of the image is very good and better than that in some previous studies [22]. The Gaussian beam profile and relatively high contrast of the YDS interference fringes confirm that the HHG radiation is highly coherent. The fringe contrast is low ( $<0.5$ ) for the YDS (50  $\mu\text{m}$  separation) and very low ( $<0.1$ ) for the YDS (75  $\mu\text{m}$  separation), as shown in Fig. 4. The resolution of the CCD may also cause a reduction in the contrast of the interference fringes from these YDSs. An extension of the distance of the CCD to the YDS is necessary for a detailed study when YDSs with 50  $\mu\text{m}$  and 75  $\mu\text{m}$  separation are used. We note instability in the beam pointing of the IR source, which will have an effect on the YDS interference pattern and therefore on the spatial coherence measurement. A beam stabilization system will be installed in the future.

### 3. Conclusion

Using infrared femtosecond driving laser pulses generated by a high-power optical parameter amplifier with a BIBO nonlinear crystal and using a semi-infinite gas cell configuration, we have demonstrated the phase-matched generation of coherent, soft x-ray, high harmonic emission around the water window region. The beam profile and spatial coherence measurements in this region, using YDS measurements, show excellent coherence characteristics of the source. This source will enable future high-resolution table-top microscopy studies of a range of nano- and biological material samples.

### References

1. M. Gisselbrecht, D. Descamps, C. Lyngå, A. L'Huillier, G. Wahlström, and M. Meyer, "Absolute photoionization cross sections of excited He states in the near-threshold region," *Phys. Rev. Lett.* **82**, 4607–4610 (1999).
2. M. Uiberacker, T. Uphues, M. Schultze, A. J. Verhoef, V. Yakovlev, M. F. Kling, J. Rauschenberger, N. M. Kabachnik, H. Schröder, M. Lezius, K. L. Kompa, H. G. Müller, M. J. J. Vrakking, S. Hendel, U. Kleineberg, U. Heinzmann, M. Drescher, and F. Krausz, "Attosecond real-time observation of electron tunnelling in atoms," *Nature* **446**, 627–632 (2007).

3. S. L. Sorensen, O. Björneholm, I. Hjelte, T. Kihlgren, G. Öhrwall, S. Sundin, S. Svensson, S. Buil, D. Descamps, A. L'Huillier, J. Norin, and C. Wahlström, "Femtosecond pump-probe photoelectron spectroscopy of predissociative Rydberg states in acetylene," *J. Chem. Phys.* **112**, 8038–8043 (2000).
4. E. Gagnon, P. Ranitovic, X. M. Tong, C. L. Cocke, M. M. Murnane, H. C. Kapteyn, and A. S. Sandhu, "Soft X-ray-driven femtosecond molecular dynamics," *Science* **317**, 1374–1378 (2007).
5. M. Bauer, C. Lei, K. Read, R. Tobey, J. Gland, M. M. Murnane, and H. C. Kapteyn, "Direct observation of surface chemistry using ultrafast soft-X-ray pulses," *Phys. Rev. Lett.* **87**, 025501 (2001).
6. A. L. Cavalieri, N. Müller, T. Uphues, V. S. Yakovlev, A. Baltuška, B. Horvath, B. Schmidt, L. Blümel, R. Holzwarth, S. Hendel, M. Drescher, U. Kleineberg, P. M. Echenique, R. Kienberger, F. Krausz, and U. Heinzmann, "Attosecond spectroscopy in condensed matter," *Nature* **449**, 1029–1032 (2007).
7. L. Miaja-Avila, C. Lei, M. Aeschlimann, J. L. Gland, M. M. Murnane, H. C. Kapteyn, and G. Saathoff, "Laser-assisted photoelectric effect from surfaces," *Phys. Rev. Lett.* **97**, 113604 (2006).
8. M. Schnürer, Ch. Strelt, P. Wobrauschek, M. Hentschel, R. Kienberger, Ch. Spielmann, and F. Krausz, "Femtosecond X-ray fluorescence," *Phys. Rev. Lett.* **85**, 3392–3395 (2000).
9. D. Descamps, C. Lyng, J. Norin, A. L'Huillier, C.-G. Wahlström, J.-F. Hergott, H. Merdji, P. Salieres, M. Bellini, and T. W. Hänsch, "Extreme ultraviolet interferometry measurements with high-order harmonics," *Opt. Lett.* **25**, 135–137 (2000).
10. P. Salieres, L. Le Déroff, T. Auguste, P. Monot, P. d'Oliveira, D. Campo, J. F. Hergott, H. Merdji, and B. Carré, "Frequency-domain interferometry in the XUV with high-order harmonics," *Phys. Rev. Lett.* **83**, 5483–5486 (1999).
11. S. Dobosz, G. Doumy, H. Stabile, P. D'Oliveira, P. Monot, F. Réau, S. Hüller, and Ph. Martin, "Probing hot and dense laser-induced plasmas with ultrafast XUV pulses," *Phys. Rev. Lett.* **95**, 025001 (2005).
12. B. Chen, R. A. Dilanian, S. Teichmann, B. Abbey, A. G. Peele, G. J. Williams, P. Hannaford, L. V. Dao, H. M. Quiney, and K. A. Nugent, "Multiple wavelength diffractive imaging," *Phys. Rev. A* **79**, 023809 (2009).
13. T. Gorniak, R. Heine, A. P. Mancuso, F. Staier, C. Christophis, M. E. Pettitt, A. Sakdinawat, R. Treusch, N. Guerassimova, J. Feldhaus, C. Gutt, G. Grübel, S. Eisebitt, A. Beyer, A. Götzhäuser, E. Weckert, M. Grunze, I. A. Vartanyants, and A. Rosenhahn, "X-ray holographic microscopy with zone plates applied to biological samples in the water window using 3rd harmonic radiation from the free-electron laser FLASH," *Opt. Express* **19**, 11059–11070 (2011).
14. A. Rundquist, C. G. Durfee, Z. Chang, C. Herne, S. Backus, M. M. Murnane, and H. C. Kapteyn, "Phase-matched generation of coherent soft X-rays," *Science* **280**, 1412–1415 (1998).
15. K. O'Keeffe, T. Robinson, and S. M. Hooker, "Quasi-phase-matching high harmonic generation using trains of pulses produced using an array of birefringent plates," *Opt. Express* **20**, 6236–6247 (2012).
16. E. Takahashi, Y. Nabekawa, T. Otsuka, M. Obara, and K. Midorikawa, "Generation of highly coherent submicrojoule soft x-rays by high-order harmonics," *Phys. Rev. A* **66**, R21802 (2002).
17. C. G. Durfee, A. R. Rundquist, S. Backus, C. Herne, M. M. Murnane, and H. C. Kapteyn, "Phase matching of high-order harmonics in hollow waveguides," *Phys. Rev. Lett.* **83**, 2187–2190 (1999).
18. E. Seres, J. Seres, F. Krausz, and C. Spielmann, "Generation of coherent soft-x-ray radiation extending far beyond the titanium L edge," *Phys. Rev. Lett.* **92**, 163002 (2004).
19. E. J. Takahashi, T. Kanai, K. L. Ishikawa, Y. Nabekawa, and K. Midorikawa, "Coherent water window x-ray by phase-matched high-order harmonic generation in neutral media," *Phys. Rev. Lett.* **101**, 253901 (2008).
20. P. Colosimo, G. Doumy, C. I. Blaga, J. Wheeler, C. Hauri, F. Catoire, J. Tate, R. Chirila, A. M. March, G. G. Paulus, H. G. Müller, P. Agostini, and L. F. DiMauro, "Scaling strong-field interactions towards the classical limit," *Nat. Phys.* **4**, 386–389 (2008).

21. T. Popmintchev, M.-C. Chen, O. Cohen, M. E. Grisham, J. J. Rocca, M. M. Murnane, and H. C. Kapteyn, "Extended phase matching of high harmonics driven by mid-infrared light," *Opt. Lett.* **33**, 2128–2130 (2008).
22. M.-C. Chen, P. Arpin, T. Popmintchev, M. Gerrity, B. Zhang, M. Seaberg, D. Popmintchev, M. M. Murnane, and H. C. Kapteyn, "Bright, coherent, ultrafast soft x-ray harmonics spanning the water window from a tabletop light source," *Phys. Rev. Lett.* **105**, 173901 (2010).
23. C. Vozzi, F. Calegari, E. Benedetti, S. Gasilov, G. Sansone, G. Cerullo, M. Nisoli, S. D. Silvestri, and S. Stagira, "Millijoule-level phase-stabilized few-optical-cycle infrared parametric source," *Opt. Lett.* **32**, 2957–2959 (2007).
24. M. Nisoli, S. De Silvestri, V. Magni, O. Svelto, R. Danielius, A. Piskarskas, G. Valiulis, and A. Varanavicius, "Highly efficient parametric conversion of femtosecond Ti:sapphire laser pulses at 1 kHz," *Opt. Lett.* **19**, 1973–1975 (1994).
25. K. R. Wilson and V. V. Yakovlev, "Ultrafast rainbow: tunable ultrashort pulses from a solid-state kilohertz system," *J. Opt. Soc. Am. B* **14**, 444–448 (1997).
26. E. J. Takahashi and K. Midorikawa, "Water window high harmonic x-ray lasers," *Proc. SPIE* **7451**, 745102 (2009).
27. O. D. Mücke, S. Ališauskas, A. J. Verhoef, A. Pugžlys, A. Baltuška, V. Smilgevičius, J. Pocius, L. Giniunas, R. Danielius, and N. Forget, "Self-compression of millijoule 1.5  $\mu\text{m}$  pulses," *Opt. Lett.* **34**, 2498–2500 (2009).
28. H. Hellwig, J. Liebertz, and L. Bohaty, "Exceptional large nonlinear optical coefficients in the monoclinic bismuth borate BiB<sub>3</sub>O<sub>6</sub> (BIBO)," *Solid State Commun.* **109**, 249–251 (1998).
29. P. Tzankov and V. Petrov, "Effective second-order nonlinearity in acentric optical crystals with low symmetry," *Appl. Opt.* **44**, 6971–6985 (2005).
30. V. Petrov, F. Noack, P. Tzankov, M. Ghotbi, M. Ebrahim-Zadeh, I. Nikolov, and I. Buchvarov, "High-power femtosecond optical parametric amplification at 1 kHz in BiB<sub>3</sub>O<sub>6</sub> pumped at 800 nm," *Opt. Express* **15**, 556–563 (2007).
31. L. V. Dao, S. Teichmann, J. Davis, and P. Hannaford, "Generation of high flux, highly coherent extreme ultraviolet radiation in a gas cell," *J. Appl. Phys.* **104**, 023105 (2008).
32. Lawrence Berkeley National Library, "Filter transmission," [http://henke.lbl.gov/optical\\_constants/filter2.html](http://henke.lbl.gov/optical_constants/filter2.html).
33. J. Tate, T. Auguste, H. G. Muller, P. Salieres, P. Agostini, and L. F. DiMauro, "Scaling of wave-packet dynamics in an intense midinfrared field," *Phys. Rev. Lett.* **98**, 013901 (2007).
34. V. Tosa, E. Takahashi, Y. Nabekawa, and K. Midorikawa, "Generation of high-order harmonics in a self-guided beam," *Phys. Rev. A* **67**, 063817 (2003).
35. E. Constant, D. Garzella, P. Breger, E. Mével, Ch. Dorrer, C. Le Blanc, F. Salin, and P. Agostini, "Optimizing high harmonic generation in absorbing gases: model and experiment," *Phys. Rev. Lett.* **82**, 1668–1671 (1999).